

Combination of a multi-organ microphysiological system (MO-MPS) and a pharmacokinetic-pharmacodynamic (PK-PD) model to evaluate drug-drug interactions (DDI)

Kenta Shinha¹, Tatsuto Ono¹, Ryota Nakazato¹, and Hiroshi Kimura¹

¹Tokai University - Shonan Campus

May 5, 2020

Abstract

In the field of drug discovery, the emergence of unexpected toxicity is often a problem resulting from a poor understanding of the pharmacokinetics of drug-drug interactions (DDI). In this context, “organs-on-a-chip” has been proposed as a novel *in vitro* model to evaluate drug efficacy and toxicity in pharmacology, but it has not yet been applied to DDI research. Here, we aim to first estimate a drug-specific parameter, namely, extraction ratio, using a multi-organ microphysiological system (MO-MPS) and to subsequently evaluate the DDI using a pharmacokinetic-pharmacodynamic (PK-PD) model. For this, we propose a combination of an MO-MPS, with a liver part as a metabolic model and a cancer part as a drug target model, and its corresponding PK-PD model. The results of the DDI effects evaluated, thus, were consistent with those previously reported, confirming the efficacy of the combination of an MPS and a PK-PD model in DDI research. It is possible to evaluate more clearly, the effect of the concomitantly administered drugs on the pharmacokinetic changes occurring in MPS, by evaluating DDI by the PK-PD model, using parameters inferred from the experimental results. Our proposed method could facilitate both, a better understanding of the pharmacokinetic mechanisms with DDI as also the evaluation of organ-organ interactions using multi-organ MPS.

Introduction

New medicines are approved and manufactured following basic research, nonclinical tests, and clinical tests. The efficacy and toxicity of the drug candidate compounds are evaluated in both nonclinical and clinical tests. However, toxicities not observed in clinical trials may appear after the medicines are sold. For example, serious side effects of the combination of sorivudine and 5-fluorouracil were reported in the 1990s after sorivudine was made available for medical consumption. These unexpected toxicities are due to drug-drug interactions (DDI) caused by the concomitant administration of multiple drugs for effective healing. (Diasio, (1998)) All of the countless combinations of the new drugs with other drugs are impossible to be evaluated during pre-production testing. Therefore, a detailed understanding of pharmacokinetics with DDI is necessary to reduce the risks associated with drug combinations. (Beijnen and Schellens, (2004)) However, due to the species difference between experimental animals and human, experimental animals cannot adequately reproduce the reactions on humans. Therefore, it becomes difficult to accurately predict and understand the pharmacokinetics of drug-drug interactions in the human body through animal testing. (Dehne et al., (2017))

To address this, pharmacokinetic (PK) models have been actively utilized. The prediction of pharmacokinetics *in vivo* is made possible by mathematical models of variability over time of drug concentration through absorption, distribution, metabolism, excretion, and accumulation in tissues and cohesion with drug proteins. Furthermore, efficacy and toxicity can be predicted effectively from the drug dose by combining PK and pharmacodynamic (PD) models (PK-PD), thereby representing the relationship between drug concentration and

physiological effects.(Abaci and Shuler, (2015)) A PK–PD model is established based on drug-specific parameters obtained from *in vitro* tests using cultured cells and microsomes and then evaluated by comparing with results of animal and clinical tests.(Prantil-Baum et al., (2018)) However, data from clinical tests are limited to concentrations of the compounds, metabolites in blood or excreta, drug efficacy to disease, and side effects. Additionally, the drug accumulation in organs and tissues and physiological efficacy such as activation and deactivation could be evaluated by animal tests. However, the detailed evaluation of pharmacokinetics remains challenging because data from animal tests are discrete, and it is difficult to continuously observe the efficacy and drug concentration. Regarding *in vitro* tests using cultured cells, *in vivo* environments are not sufficiently reproduced, and the co-culture of multiple organ model cells is challenging. Therefore, novel cell-based assay systems, which supplement conventional *in vitro* tests and animal tests, are essential for the accurate prediction and increased understanding of pharmacokinetics of DDI.(Ishida, (2018))

Microfluidics-based *in vitro* culture models such as organs-on-a-chip (OsoC) and microphysiological systems (MPS) have recently been considered as novel cell-based assay systems for pharmacokinetic research.(Bhatia and Ingber, (2014); Esch et al., (2015); Marx et al., (2017)) To evaluate organ interactions *in vitro*, several organ model cells are cultured in different compartments connected by microchannels on MPS. Parameters of MPS, such as flow ratio between organ models, residence time of circulating medium in the organ parts, and ratio of the cell number to medium volume, accommodate the PK model by the design of microchannels.(Abaci and Shuler, (2015)) Therefore, MPS may be useful to evaluate the PK model and examine drug-specific physiological effects.(Lee et al., (2017)) The usefulness of combining the PK model and MPS has been demonstrated by the consistency between the drug concentration calculations obtained from the PK model and the experimental results obtained using MPS.(Sung et al., (2010)) In addition, the calculated parameters using MPS experimental results were more similar to those of *in vivo* than to those of conventional *in vitro* tests.(Lee et al., (2019)) The combination of the PK model and MPS has also been useful for research involving not only drugs but also substances, such as glucose, in the body.(Lee et al., (2019)) However, previous studies have not undertaken the study of concomitant administration with multi drugs using MPS; thus, the usefulness for DDI studies using PK models and MPS has yet to be shown. Therefore, we estimated drug-specific parameters such as extraction ratios and subsequently evaluated the changes in drug efficacy due to DDI. We demonstrate the usability of the combination of the PK model and MPS in this DDI study. We further propose a multi-organ microphysiological system (MO–MPS), with a liver part as the metabolic model and a cancer part as the drug target model, and a PK–PD model describing the MO–MPS. A prodrug, CPT-11, was used to evaluate the drug efficacy of the metabolite in the liver part of the MPS. Drug-specific parameters were estimated by using the proposed PK–PD model from the results of drug efficacy tests by varying the flow ratio to liver part and lung cancer part in the MPS. The DDI were evaluated by comparing the results of the concomitant administration experiment using the MPS and the results of simulation using the proposed PK–PD model with the estimated parameters. We found that it was possible to evaluate and understand DDI by comparing the results of the PK-PD model and the MO-MPS.

Materials and Methods

2.1 Development of the multi-organ microphysiological system (MO–MPS)

We developed a multi-organ microphysiological system (MO–MPS) integrated with a liver part having metabolic functions based on pharmacokinetics and a lung cancer part as a drug target. The blood *in vivo* is dispensed to the organs by the heart after assimilating the oxygen from the lung. The blood flow ratio between liver, heart, and lung is 1:3.3:3.3(Fig. 1A).(Takahashi, (1989)) A stirrer-based micropump, which we had developed previously, was integrated for medium perfusion on the MO–MPS.(Nakayama et al., (2014)) The flow ratio was controlled by the resistance of a bypass-channel installed onto the MO–MPS to be similar *in vivo* (Fig. 1B). The design of the bypass channel was optimized using ANSYS 17.1 (ANSYS Inc., USA), a fluidic simulation software by the finite element method (Fig. 1C). The dimensions of the chambers of the lung and the liver cancer parts were 15 mm² and 50 mm², respectively. The height of the channel and cell culture chambers were 380 μm and 770 μm, respectively.

The MO–MPS was fabricated by conventional photolithography and soft lithography methods.(McDonald

and Whitesides, (2002)) A chromium mask for photolithography, which was used to fabricate microstructure, was designed using a computer-aided design software (AutoCAD, Autodesk, USA) and fabricated using a micro-pattern generator (μ PG101, Heidelberg instruments Inc., Germany). A negative photoresist (SU-8 2010, MicroChem Corp., USA) was spin-coated onto a silicon wafer. After baking, the microchannel pattern was formed on the substrate using ultraviolet lamp. The stepped structures of the microchannels and the cell culture chambers were fabricated similarly. The substrate was used as a master mold for polydimethylsiloxane (PDMS, SILPOT 184, Dow Corning Toray, Japan), the material of the MO-MPS. A 10:1 mixture of PDMS and a polymerization agent was poured onto the master mold and heat cured in an oven at 75 @C for 2 h. The cured PDMS was peeled from the master mold to produce a PDMS chip as to which the channel pattern was transferred. The surface of the PDMS was coated with CYTOP (CTL-107MK, AGC, Japan) to spin the stirrer bar smoothly. A 7% CYTOP solution was casted onto the micropump chamber and baked at 65 for 30 min and 100 for 60 min. The PDMS surfaces were activated using a plasma cleaner (PDC-32G, Harrick Plasma, USA). After setting the stirrer bar into the chamber, the MO-MPS was assembled to permanently bond the PDMS chips (Fig. 1D).

2.2 Flow characterization of the MO-MPS

Flow velocity was measured by the particle tracking velocimetry (PTV) method using fluorescent microbeads with a diameter of 1.17 μ m (17687, Polysciences, USA). The fluorescent microbeads were suspended in ultra-pure water with Tween20 (103168, MP Biomedicals, USA). After filling the microchannels, the suspension was perfused by the stirrer-based micropump at between 1300 and 2800 rpm. The flowing microbeads in the microchannels were observed by a high-speed camera (MEMRECAM HX-3, nac Image Technology Inc., Japan) installed into a fluorescence microscope (IX71, Olympus, Japan). The flow rates in each organ were calculated from the velocities of the flowing fluorescent bead measured using ImageJ.

2.3 Cell culture

HepG2 (JCRB1054, JCRB Cell Bank, Japan) was used as a liver model cell for metabolic functions, whereas A549 (RCB0098, RIKEN BRC, Japan) was used as a cancer model cell. The cells were cultured at 37 @C in an incubator in a humidified atmosphere containing 5% CO₂. Dulbecco's Modified Eagle Medium supplemented with 10% fetal bovine serum (FBS, Bio West, Japan), 1% non-essential amino acid solution (11140-050, Thermo Fisher, USA), and 1% antibiotic antimycotic solution (161-23181, FUJIFILM Wako, Japan) was used as culture media for both cells.

Cell inoculation and cell culturing were performed within the MO-MPS according to the following procedure. The cell culture chambers in the MO-MPS were coated with collagen type I-P (634-00663, Nitta Gelatin Inc., Japan) as an extracellular matrix (ECM). The collagen was chemically bonded to PDMS through 3-aminopropyltriethoxysilane (aminosilane, KBE-903, Shin-Etsu Chemical Co., Ltd., Japan) and glutaraldehyde (GAD, 17026-32, KANTO CHEMICAL CO., INC., Japan) that were coated to the bottom surface of the cell culture chambers. (Chuah et al., (2015)) After the permanent bonding of PDMS chips, the cell culture chambers were coated with aminosilane by immediately removing the aminosilane after its introduction and allowing to stand at 54 for 2 h. Then, 2.5% glutaraldehyde was introduced to the microchannel and allowed to stand at room temperature for 1 h. Finally, the microchannel was filled with 0.1 mg/mL collagen type I-P and allowed to stand at 4 for 12 h. The microchannel was washed by ultra-pure water after coating with aminosilane and glutaraldehyde and by phosphate-buffered saline (PBS) after collagen coating. HepG2 cells were seeded into the liver part chamber at $1.7\text{--}2.0 \times 10^5$ cells/cm². After prior culture for 48 h, the A549 cells were seeded into the lung cancer part chamber at $1.7\text{--}2.0 \times 10^4$ cells/cm² and cultured for 24 h. The culture medium in the MO-MPS was exchanged daily.

2.4 Establishment of the PK-PD model

A PK-PD model was established by combining a separately constructed PK model and a PD model. The PK model is a mathematical model showing time-dependent changes in concentrations of drug and biological matter, whereas the PD model shows the relationship between drug efficacy and drug concentration. The PK-PD model is used to predict the drug efficacy on the target site using the drug dosage. However, alternative

indices of drug concentration are needed in models involving drug concentration changes over time because the PD model expresses drug efficacy as a function of the drug concentration. Normally, the area under the concentration–time curve (AUC) is used as an alternative index to drug concentration and is an integral value of a drug concentration–time function as it represents the full drug dose *in vivo* in pharmacokinetics study.

We established a PK–PD model that predicts the drug efficacy on the lung cancer part from values of the AUC obtained by the PK model. The microchannel volume of the MO–MPS and changes in the drug concentration in the organ parts must be considered because pharmacokinetics depends on the drug concentration in each organ part and the metabolism of compounds by these organs (Fig. 1E). Only the metabolism of the liver part was considered in the proposed model because the number of metabolic enzymes in the lung cancer part, the drug target part, was considerably lower than that of the liver. The gradient of the prodrug concentration is expressed as follows:

$$\frac{d[C_P]}{dt} = -k_P [C_P] \quad (1)$$

where k_P is the elimination rate constant of the prodrug. The change in prodrug concentration is as follows:

$$C_P [t] = X_0 \times e^{-k_P \times t} \quad (2)$$

where X_0 is the initial concentration of the prodrug.

The concentrations of the metabolites simultaneously increase because of prodrug metabolism and decrease because of metabolic enzyme reactions. The metabolites are different due to species of enzymes that metabolize prodrugs. Therefore, the rate at which the metabolic enzyme contributes to the overall metabolism must be considered. The gradient of each metabolite concentration can be expressed by:

$$\frac{d[C_M]}{dt} = fm \times k_P [C_P] - k_M [C_M] \quad (3)$$

where km is the elimination rate constant of the metabolite; and fm is the fraction metabolized defined as the metabolized rate by each metabolic enzyme. The change in metabolite concentration then becomes as follows:

$$C_M [t] = \frac{k_P \times fm \times X_0}{k_P - k_M} \times (e^{-k_M \times t} - e^{-k_P \times t}) \quad (4)$$

The elimination rate constants can be expressed as:

$$k = \frac{CL}{V_d} = \frac{Q \times E}{V_d} \quad (5)$$

where CL is the clearance in the liver part [$\mu\text{L}/\text{h}$]; V_d is the distribution volume [μL]; Q is the flow rate in the liver part; and E is the extraction ratio in the liver part. The change in metabolite concentration can be expressed as:

$$C_M [t] = \frac{E_P \times fm \times X_0}{E_P - E_M} \times \left(e^{-\frac{Q \times E_M}{V_d} \times t} - e^{-\frac{Q \times E_P}{V_d} \times t} \right) \quad (6)$$

A PD model was developed based on the drug efficacy of SN-38, whose concentration was evaluated previously, on A549 cells. (Mijatovic et al., (2006)) SN-38, metabolite of CPT-11 used in this study, has strong anticancer effect. The drug efficacy is expressed as:

$$\frac{\text{Cell density}}{\text{Control cell density}} = -0.086 \times \ln(\text{Auc}) + 0.512 \quad (7)$$

AUC [$\text{h}[\text{?}]\text{ng}/\mu\text{L}$] is an integral part of the concentration change function. Therefore, the drug efficacy after t hours from the administration of drug dose can be expressed as:

$$\frac{\text{Cell density}}{\text{Control cell density}} = -0.086 \times \ln \left(\int_t^0 C_M [t] \right) + 0.512 \quad (8)$$

2.5 Estimating drug efficacy-specific parameters in the PK–PD model

An unknown parameter, the extraction ratio in the liver part E , in the PK–PD model must be experimentally estimated using the MO–MPS. Drug efficacy tests using two different types of the MO–MPS with different

flow rates in the liver part were carried out. CPT-11 (2688, Tocris Bioscience, UK), an anticancer drug widely used in the treatment of alveolus and large intestine cancers, was used as a drug model. Two types of the MO-MPS with and without the bypass channel that have 1:3.3 physiological flow ratio (liver:lung cancer part) and 1:1 non-physiological flow ratio (liver:lung cancer part), respectively, were used to evaluate how flow ratio influences drug efficacy on the MO-MPS. The cells were exposed to 15 μM CPT-11 dissolved in the culture medium, which was exchanged every 24 h. After exposure for 72 h, the cells were stained by hoechst33342 (346-07951, Dojindo Laboratories, Japan) and observed using a CCD camera (DP72, Olympus Corporation, Japan) installed with a fluorescence microscope. The drug effect was evaluated using the density of the A549 cells measured from the fluorescent images. The extraction ratios in the liver part of CPT-11 and SN-38 in the MO-MPS were estimated from the experimental results using the MO-MPS with and without bypass channels and our PK-PD model using Eq. (8).

2.6 Evaluation of drug-drug interaction

A DDI evaluation experiment using the MO-MPS was carried out using CPT-11 and either simvastatin (SV, S0509, Tokyo Chemical Industry Co., Ltd., Japan), a lipid-lowering drug, or ritonavir (RTV, R0116, Tokyo Chemical Industry Co., Ltd., Japan), an anti-HIV drug, to effect metabolic functions change on the MO-MPS. The metabolism of CPT-11 to SN-38 would be decreased by the concomitant administration of SV, which is an inhibitor of carboxylesterase2 (CES2). (Shen et al., (2019)) We expect that the concomitant administration of CPT-11 and RTV, which is an inhibitor of cytochrome P450 3A4 (CYP3A4), would not affect the amount of SN-38 in the MO-MPS because CYP3A4 expression on HepG2 is quite low. (Huch et al., (2015)) CPT-11 concentration was 15 μM , whereas SV concentration was 1 μM , which makes CES2 expression to be 50%. (Fukami et al., (2010)) Because RTV concentration was 10 μM , the CYP3A4 expression of microsomes from the human liver becomes 5%. (Eagling et al., (1997)) The culture medium in the MO-MPS was exchanged every 24 h. After 72 h, cell densities were observed as previously mentioned. The effects of DDI on pharmacokinetics were evaluated by comparing the predicted cell density of the PK-PD model with that of the experimental results.

2.7 Statistical Analysis

All values are expressed as mean \pm S.D. of experiments performed in at least triplicates. Unpaired Tukey HSD test was performed for the statistical evaluation, and differences were statistically significant when $p < 0.05$.

Result and Discussion

3.1 Flow characterization of the MO-MPS

The flow rate in the organ parts increased with increasing rotation speed of the stirrer-based micropump (Fig. 2A). The flow ratio was stabilized, and physiological blood flow ratio of 3.3 was achieved at more than 1,900 rpm (Fig. 2B).

The increase in flow rate is due to an increase in the amount of liquid pushed out in the similar direction as the flow as caused by increasing rotational speed of the stirrer-based micropump. The physiological flow ratio could not be replicated when the stirrer-based micropump rotational speed was less than 1,600 rpm, and the dispersion of the flow ratio was slightly large when the speed was less than 1,900 rpm. These results suggest that the flow in the MO-MPS would be stable when the rotational speed of the stirrer-based micropump is above 1,900 rpm. A previous study reported that the flow is unsteady when the stirrer-based micropump rotational speed is below 500 rpm, whereas the flow rate increases linearly when the rotation speed is at least 500 rpm. (Kimura et al., (2008)) Our obtained flow rate was lower, whereas the rotational speeds we needed to stabilize the flow rate were higher than those of previous study. The flow from the stirrer-based micropump depends on the flow resistance of a microchannel. The channel's resistance was higher than that of the previous device; therefore, the amount of the liquid pushed out by stirrer was smaller. The range of flow rate is limited by the channel resistance, although the stirrer-based micropump is suitable for evaluating organ-organ interactions because the culture medium volume can be reduced, and continuous

stable perfusion is possible. Therefore, the rotational speed of the stirrer-based micropump was set at 2,800 rpm in consideration of the flow ratio and flow stability in our experiments.

3.2 Estimation of the extraction ratio in the liver part by the drug efficacy test using the MO-MPS

The density ratios of A549 cells exposed to CPT-11 for 72 h on the MO-MPS with and without bypass channels decreased significantly to 33.2% and 25.6%, respectively, as compared to that of the control, i.e., not exposed to CPT-11 (Fig. 3A) with a significant difference between the MO-MPS with and without bypass channels.

Prodrugs are primarily metabolized by metabolic enzymes in the liver, following which, the metabolites distributed by blood flow, show the drug effects and side effects on tissues and organs *in vivo*. CPT-11 is metabolized mainly by CES2 and CYP3A4, which are metabolic enzymes in hepatocytes (Fig. 3C). (Ma et al., (2000); Mullangi et al., (2010)) CPT-11 is metabolized to inactive metabolites (i.e., APC and NPC), which do not have anticancer effects, by CYP3A4, whereas it is metabolized to SN-38, which has approximately 1,000 times the anticancer effect of CPT-11, by CES2. (Uchida et al., (2013)) SN-38 exhibits strong anticancer effect by inhibiting the activity of Type-1 topoisomerase, which is necessary for cell proliferation. (Kurita and Kaneda, (1999)) Moreover, SN-38 is conjugated by UDP-glucuronosyltransferase 1A1 (UGT1A1) to yield SN-38G, which is inert, and thereby has no anticancer activity. (ref) The significant decrease in the density ratio of the A549 cells exposed to CPT-11 indicates that CPT-11 was metabolized by the HepG2 cells, and Type-1 topoisomerase were subsequently inhibited by SN-38. The cell density ratio of the MO-MPS with the bypass channel was significantly higher than that without the bypass channel because the AUC of SN-38 on the MO-MPS with bypass channel did not increase due to the decline in clearance, which indicates the ability to remove drugs by metabolism, in the liver part with lower flow rate.

The AUC of SN-38 were obtained from the cell density ratio in the drug efficacy test using the PD model (eq. 7). Then, the extraction ratios of both CPT-11 and SN-38 in the liver part were estimated by AUC of SN-38 and the PK model (eq. 6). The expression level of CYP3A4 in HepG2 is extremely low, (Levy et al., (2015); Wilkening et al., (2003)) and CPT-11 is only metabolized to SN-38 by CES2. Therefore, the $f_{m_{CES2}}$, which represents the fraction of metabolism of CPT-11 by CES2, was set to 1.0. We have assumed that the metabolism of SN-38 to SN-38G is nonreversible in the PK-PD model because SN-38G does not convert to SN-38 in the MO-MPS. SN-38G normally changes by conjugation with β -glucuronidase on intestinal bacteria *in vivo*. V_d was defined as the volume of the microchannel on the MO-MPS because the compound does not effuse outside. The AUCs of SN-38 were calculated to be $8.15 h \bullet ng/uL$ and $19.63h \bullet ng/uL$ on the MO-MOP with and without the bypass channel, respectively (Fig. 3B). The extraction ratios of CPT-11 and SN-38 in the liver part were estimated to be 0.4% and 8.4%, respectively. When human liver microsomes were exposed to CPT-11, SN-38G was generated approximately 17 times more than the amount of SN-38, (Van Der Bol et al., (2011)) suggesting that the fraction of SN-38 metabolized to SN-38G per unit time is larger than the fraction of CPT-11 metabolized to SN-38 per unit time. The same observation was made in HepG2 model cells.

3.3 Evaluation of drug-drug interaction

Drug efficacy was predicted using the PK-PD model and the estimated extraction ratios in the liver part. The extraction ratio of CPT-11 in the liver part in concomitant administration of SV was set to 0.2% because the CES2 expression would be half. On the other hand, the extraction ratio of CPT-11 in the liver part in concomitant administration of RTV was set to 0.4%, which is the same value as that without concomitant administration, because CYP3A4 expression is extremely low in HepG2, and CYP3A4 inhibition may be no effect on pharmacokinetics. The extraction ratio of SN-38 in the liver part was set to 8.4%. A549 cells density ratios exposed to CPT-11 for 72 h without metabolic inhibitors, with RTV, and with SV were predicted to be 35.5%, 35.5% and 25.6%, respectively, of the control, i.e., no drugs (Fig. 4A). Meanwhile, their experimental values using the MO-MPS were 29.5%, 20.3% and 38.8%, respectively. The cell density ratio with SV is significantly higher than that without metabolic inhibitors. No statistically significant difference was observed between without metabolic inhibitor and with RTV although cell density with RTV

was lower than that without metabolic inhibitor (Fig. 4B).

Drug efficacy declined in the concomitant administration of SV because SV suppresses CES2 expression, which metabolizes CPT-11 to SN-38. As expected, drug efficacy did not change in the concomitant administration of RTV, which was used as CYP3A4 inhibitor, because CYP3A4 expression on HepG2 is quite low. However, drug efficacy in concomitant administration of RTV was markedly increased in the experiment. SN-38 metabolism to SN-38G is decreased by the concomitant administration of anti-HIV drugs, suggesting that anti-HIV drugs impact the metabolism by UGT1A1.(Corona et al., (2008)) HepG2 has low levels of CYP3A4 activity but still express UGT1A1.(Westerink and Schoonen, (2007)) The increase in drug efficacy may have been caused by the inhibition of UGT1A1 because the AUC of SN-38 increased by the inhibition of not only CPT-11 metabolism to APC and NPC but also SN-38 metabolism to SN-38G. Our findings involving DDI of inhibitor chemicals were quite similar to the results of previous studies, indicating that the DDI evaluation using PK-PD model and MPS is useful.

Conclusion

Although MPS is useful for pharmacokinetic studies, it has not yet been applied to DDI studies. Here, we proposed a series of DDI evaluation methods using an MPS and a PK-PD model, and demonstrated their usefulness. We established a microfluidics-based MO-MPS and its PK-PD model. From the experimental results using CPT-11, we confirmed that the MO-MPS could be used to evaluate the effect of metabolites on a drug target model. Drug-specific parameters were estimated from the PK-PD model and from the experimental results using the MO-MPS. DDI was evaluated by comparing the calculated drug efficacy of the anti-cancer drug by the PK-PD model with experimental results obtained using metabolism inhibitor. The effect of concomitantly administered drugs on the pharmacokinetic changes occurring in MPS can be more clearly identified by evaluating DDI by the PK-PD model, using parameters inferred from the experimental results. Our proposed method is useful in evaluating not only liver metabolism but also the DDI effects for different organ functions such as absorption and excretion. Furthermore, this method can be applied to the evaluation of organ-organ interaction using multi-organ MPS that reproduces enterohepatic circulation. In this study, DDI was evaluated only in terms of drug efficacy. For a more in-depth understanding of DDI, evaluating the changes in drug concentration and metabolic capacity through mathematical models and experiments is necessary. For this kind of evaluation, the contents of the culture medium and cells in the MO-MPS should be measured using liquid chromatography-mass spectrometry and PCR; we aim to perform this in our future studies. Despite this limitation, our method still proved to be valuable for the study and analysis of DDI.

Acknowledgements

This study was funded by the Program for Grant-in-Aid for Scientific Research (B) 18H01849 and the Japan Agency for Medical Research and Development (AMED).

References

- Abaci HE, Shuler ML. (2015). Human-on-a-chip design strategies and principles for physiologically based pharmacokinetics/pharmacodynamics modeling. *Integrative Biology (United Kingdom)* , 7 , 383–391. doi: 10.1039/c4ib00292j.
- Beijnen JH, Schellens JHM. (2004). Drug interactions in oncology. *Lancet Oncology* , 5 , 489–496. doi: 10.1016/S1470-2045(04)01528-1.
- Bhatia SN, Ingber DE. (2014). Microfluidic organs-on-chips. *Nature Biotechnology* , 32 , 760–772. doi: 10.1038/nbt.2989.
- Van Der Bol JM, Loos WJ, De Jong FA, Van Meerten E, Konings IRHM, Lam MH, De Bruijn P, Wiemer EAC, Verweij J, Mathijssen RHJ. (2011). Effect of omeprazole on the pharmacokinetics and toxicities of irinotecan in cancer patients: A prospective cross-over drug-drug interaction study. *European Journal of Cancer* , 47 , 831–838. doi: 10.1016/j.ejca.2010.11.030.

Chuah YJ, Kuddannaya S, Lee MHA, Zhang Y, Kang Y. (2015). The effects of poly(dimethylsiloxane) surface silanization on the mesenchymal stem cell fate. *Biomaterials Science* , 3 , 383–390. doi: 10.1039/c4bm00268g.

Corona G, Vaccher E, Sandron S, Sartor I, Tirelli U, Innocenti F, Toffoli G. (2008). Lopinavir-ritonavir dramatically affects the pharmacokinetics of irinotecan in HIV patients with Kaposi's sarcoma. *Clinical Pharmacology and Therapeutics* , 83 , 601–606. doi: 10.1038/sj.cpt.6100330.

Dehne EM, Hasenberg T, Marx U. (2017). The ascendance of microphysiological systems to solve the drug testing dilemma. *Future Science OA* , 3 , FSO185. doi: 10.4155/fsoa-2017-0002.

Diasio RB. (1998). Sorivudine and 5-fluorouracil; A clinically significant drug-drug interaction due to inhibition of dihydropyrimidine dehydrogenase. *British Journal of Clinical Pharmacology* , 46 , 1–4. doi: 10.1046/j.1365-2125.1998.00050.x.

Eagling VA, Back DJ, Barry MG. (1997). Differential inhibition of cytochrome P450 isoforms by the protease inhibitors, ritonavir, saquinavir and indinavir. *British Journal of Clinical Pharmacology* , 44 , 190–194. doi: 10.1046/j.1365-2125.1997.00644.x.

Esch EW, Bahinski A, Huh D. (2015). Organs-on-chips at the frontiers of drug discovery. *Nature Reviews Drug Discovery* , 14 , 248–260. doi: 10.1038/nrd4539.

Fukami T, Takahashi S, Nakagawa N, Maruichi T, Nakajima M, Yokoi T. (2010). In vitro evaluation of inhibitory effects of antidiabetic and antihyperlipidemic drugs on human carboxylesterase activities. *Drug Metabolism and Disposition* , 38 , 2173–2178. doi: 10.1124/dmd.110.034454.

Huch M, Gehart H, Van Boxtel R, Hamer K, Blokzijl F, Verstegen MMA, Ellis E, Van Wenum M, Fuchs SA, De Ligt J, Van De Wetering M, Sasaki N, Boers SJ, Kemperman H, De Jonge J, Ijzermans JNM, Nieuwenhuis EES, Hoekstra R, Strom S, Vries RRG, Van Der Laan LJW, Cuppen E, Clevers H. (2015). Long-term culture of genome-stable bipotent stem cells from adult human liver. *Cell* , 160 , 299–312. doi: 10.1016/j.cell.2014.11.050.

Ishida S. (2018). Organs-on-a-chip: Current applications and consideration points for in vitro ADME-Tox studies. *Drug Metabolism and Pharmacokinetics* , 33 , 49–54. doi: 10.1016/j.dmpk.2018.01.003.

Kimura H, Yamamoto T, Sakai H, Sakai Y, Fujii T. (2008). An integrated microfluidic system for long-term perfusion culture and on-line monitoring of intestinal tissue models. *Lab on a Chip* , 8 , 741–746. doi: 10.1039/b717091b.

Kurita A, Kaneda N. (1999). High-performance liquid chromatographic method for the simultaneous determination of the camptothecin derivative irinotecan hydrochloride, CPT-11, and its metabolites SN-38 and SN-38 glucuronide in rat plasma with a fully automated on-line solid-phase ext. *Journal of Chromatography B: Biomedical Sciences and Applications* , 724 , 335–344. doi: 10.1016/S0378-4347(98)00554-4.

Lee DW, Lee SH, Choi N, Sung JH. (2019). Construction of pancreas–muscle–liver microphysiological system (MPS) for reproducing glucose metabolism. *Biotechnology and Bioengineering* , 116 , 3433–3445. doi: 10.1002/bit.27151.

Lee H, Kim DS, Ha SK, Choi I, Lee JM, Sung JH. (2017). A pumpless multi-organ-on-a-chip (MOC) combined with a pharmacokinetic–pharmacodynamic (PK–PD) model. *Biotechnology and Bioengineering* , 114 , 432–443. doi: 10.1002/bit.26087.

Levy G, Bomze D, Heinz S, Ramachandran SD, Noerenberg A, Cohen M, Shibolet O, Sklan E, Braspenning J, Nahmias Y. (2015). Long-term culture and expansion of primary human hepatocytes. *Nature Biotechnology* , 33 , 1264–1271. doi: 10.1038/nbt.3377.

Ma MK, Zamboni WC, Radomski KM, Furman WL, Santana VM, Houghton PJ, Hanna SK, Smith AK, Stewart CF. (2000). Pharmacokinetics of irinotecan and its metabolites SN-38 and APC in children with

recurrent solid tumors after protracted low-dose irinotecan. *Clinical Cancer Research* , 6 , 813–819.

Marx U, Andersson TB, Bahinski A, Beilmann M, Beken S, Cassee FR, Cirit M, Daneshian M, Fitzpatrick S, Frey O, Gaertner C, Giese C, Griffith L, Hartung T, Heringa MB, Hoeng J, Jong WH De, Kojima H, Kuehnl J, Luch A, Sakharov D, Sips AJAM, Steger-hartmann T, Tagle A, Tonevitsky A, Tralau T, Tsyb S, Stolpe A Van De, Vulto P, Wang J, Wiest J, Rodenburg M, Roth A. (2017). Biology-inspired Microphysiological System Approaches to Solve the Prediction Dilemma of Substance Testing. *ALTEX* ,33 , 272–321. doi: 10.14573/altex.1603161.Biology-inspired.

McDonald JC, Whitesides GM. (2002). Poly(dimethylsiloxane) as a material for fabricating microfluidic devices. *Accounts of Chemical Research* , 35 , 491–499. doi: 10.1021/ar010110q.

Mijatovic T, De Beeck AO, Van Quaquebeke E, Dewelle J, Darro F, de Launoit Y, Kiss R. (2006). The cardenolide UNBS1450 is able to deactivate nuclear factor κ B-mediated cytoprotective effects in human non-small cell lung cancer cells. *Molecular Cancer Therapeutics* ,5 , 391–399. doi: 10.1158/1535-7163.MCT-05-0367.

Mullangi R, Ahlawat P, Srinivas NR. (2010). Irinotecan and its active metabolite, SN-38: Review of bioanalytical methods and recent update from clinical pharmacology perspectives. *Biomedical Chromatography* , 24 , 104–123. doi: 10.1002/bmc.1345.

Nakayama H, Kimura H, Fujii T, Sakai Y. (2014). Image-based evaluations of distribution and cytotoxicity of Irinotecan (CPT-11) in a multi-compartment micro-cell coculture device. *Journal of Bioscience and Bioengineering* , 117 , 756–762. doi: 10.1016/j.jbiosc.2013.11.019.

Prantil-Baun R, Novak R, Das D, Somayaji MR, Przekwas A, Ingber DE. (2018). Physiologically Based Pharmacokinetic and Pharmacodynamic Analysis Enabled by Microfluidically Linked Organs-on-Chips. *Annual Review of Pharmacology and Toxicology* , 58 , 37–64. doi: 10.1146/annurev-pharmtox-010716-104748.

Shen Y, Shi Z, Yan B. (2019). Carboxylesterases: Pharmacological Inhibition Regulated Expression and Transcriptional Involvement of Nuclear Receptors and other Transcription Factors. *Nuclear Receptor Research* , 6 . doi: 10.32527/2019/101435.

Sung JH, Kam C, Shuler ML. (2010). A microfluidic device for a pharmacokinetic – pharmacodynamic (PK – PD) model on a chip +. *Lab on a chip* , 10 , 446–455. doi: 10.1039/b917763a.

Takahashi T. (1989). *The Atlas of the Human Body*. Tokyo: Kodansha Ltd.

Uchida K, Otake K, Tanaka K, Hashimoto K, Saigusa S, Matsushita K, Koike Y, Inoue M, Ueda M, Okugawa Y, Inoue Y, Mohri Y, Kusunoki M. (2013). Clinical implications of CES2 RNA expression in neuroblastoma. *Journal of Pediatric Surgery* , 48 , 502–509. doi: 10.1016/j.jpedsurg.2012.10.004.

Westerink WMA, Schoonen WGEJ. (2007). Phase II enzyme levels in HepG2 cells and cryopreserved primary human hepatocytes and their induction in HepG2 cells. *Toxicology in Vitro* , 21 , 1592–1602. doi: 10.1016/j.tiv.2007.06.017.

Wilkening S, Stahl F, Bader A. (2003). Hepg2 With Regard To Their Biotransformation Properties. *Drug Metabolism and Disposition* ,31 , 1035–1042.

Figures

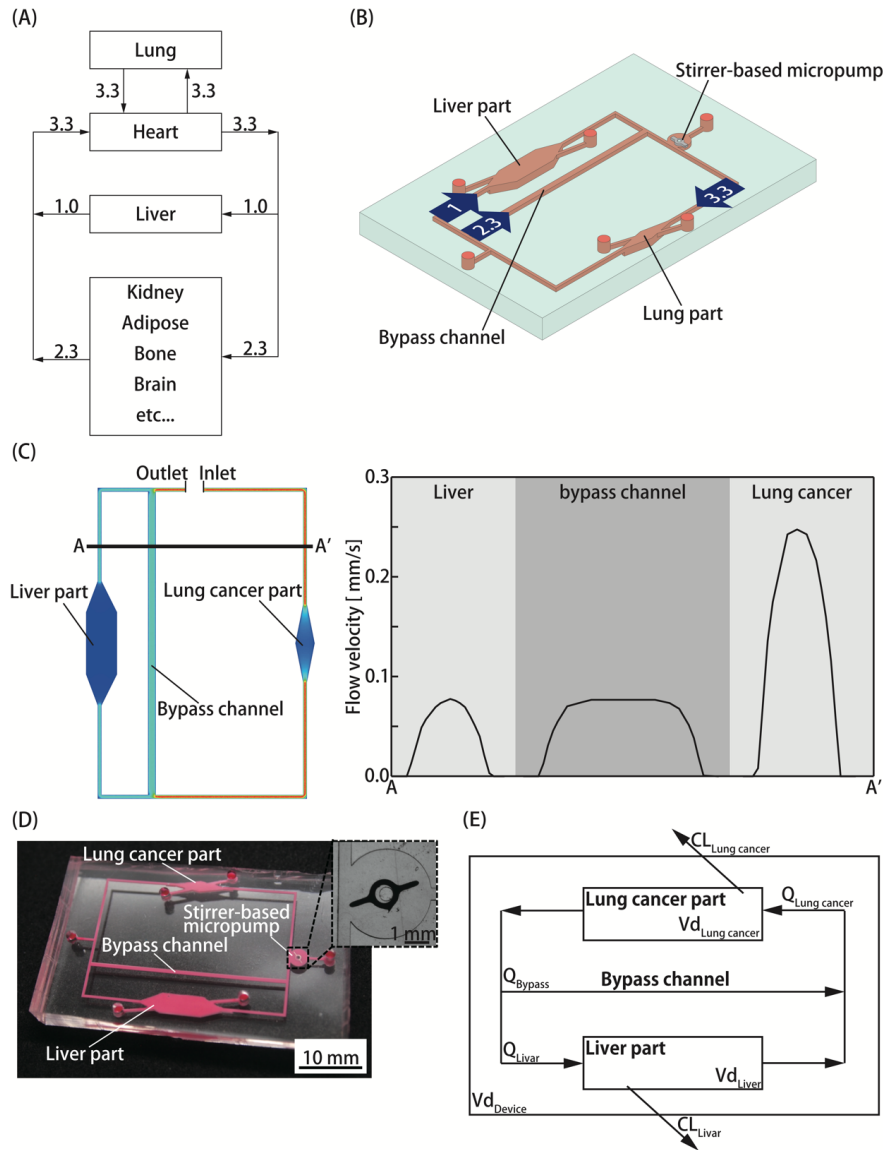


Figure 1. Physiologically-based multi-organ microphysiological system (MO-MPS). (A) Schematic of the blood flow ratio *in vivo*. After flowing into the lung, the blood is distributed to the organs by the heart. The flow ratio of the liver to the lung and heart is 1:3.3. (B) Schematic illustration of the MO-MPS. The MO-MPS consist of a liver part, a lung cancer part, and a stirrer-based micropump. The values inside the arrows are the flow rate ratios. (C) Flow velocity in the MO-MPS as estimated by ANSYS 17.1. The graph shows flow velocity on A–A' cross section. (D) Photograph of the fabricated MO-MPS with the enlarged view of the stirrer-based micropump as inset. (E) Conceptual diagram of PK model on the MO-MPS. The change in drug concentration is dependent on the flow rate and extraction ratios of organ models.

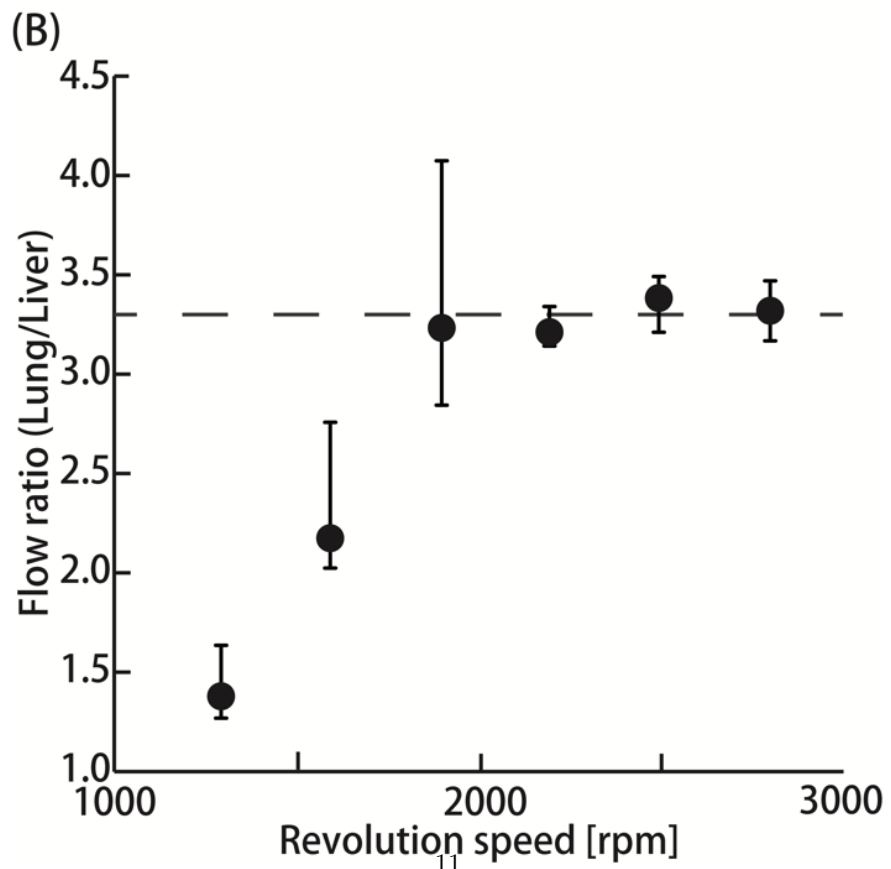
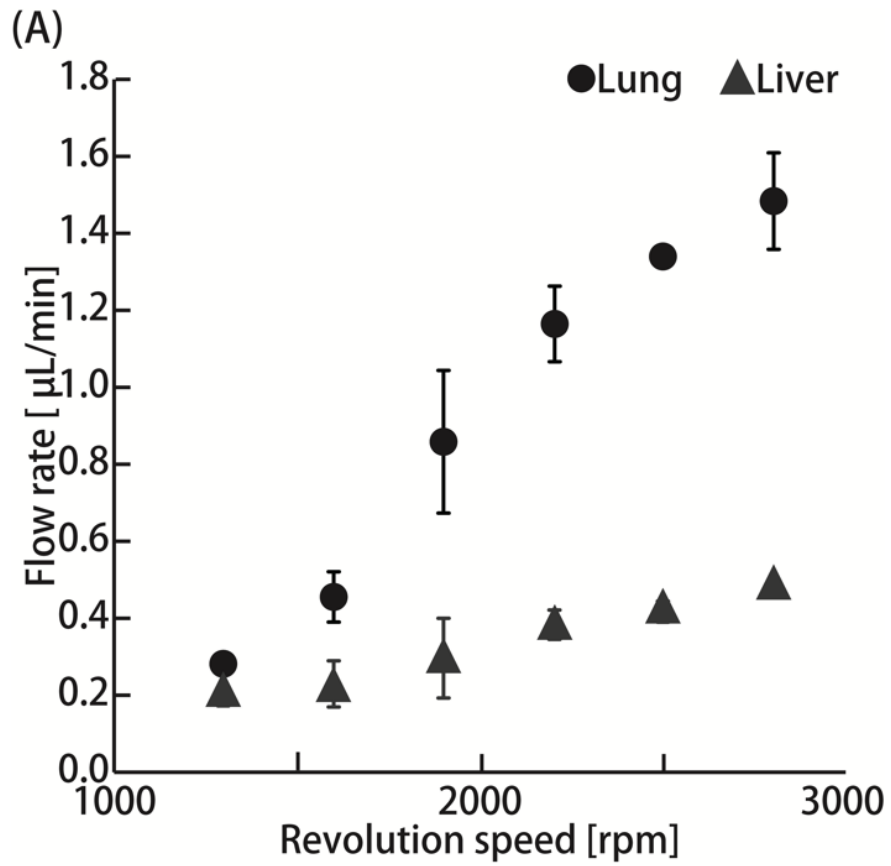


Figure 2. Flow characterization of the MO-MPS. (A) Flow rate in the liver and lung cancer parts at 1300–2800 rpm (n=3; mean± S.D.) (B) Flow ratio of the lung cancer part to liver part at 1300–2800 rpm (n=3; mean± maximum and minimum). The broken line indicates the physiological flow ratio at approximately 3.3.

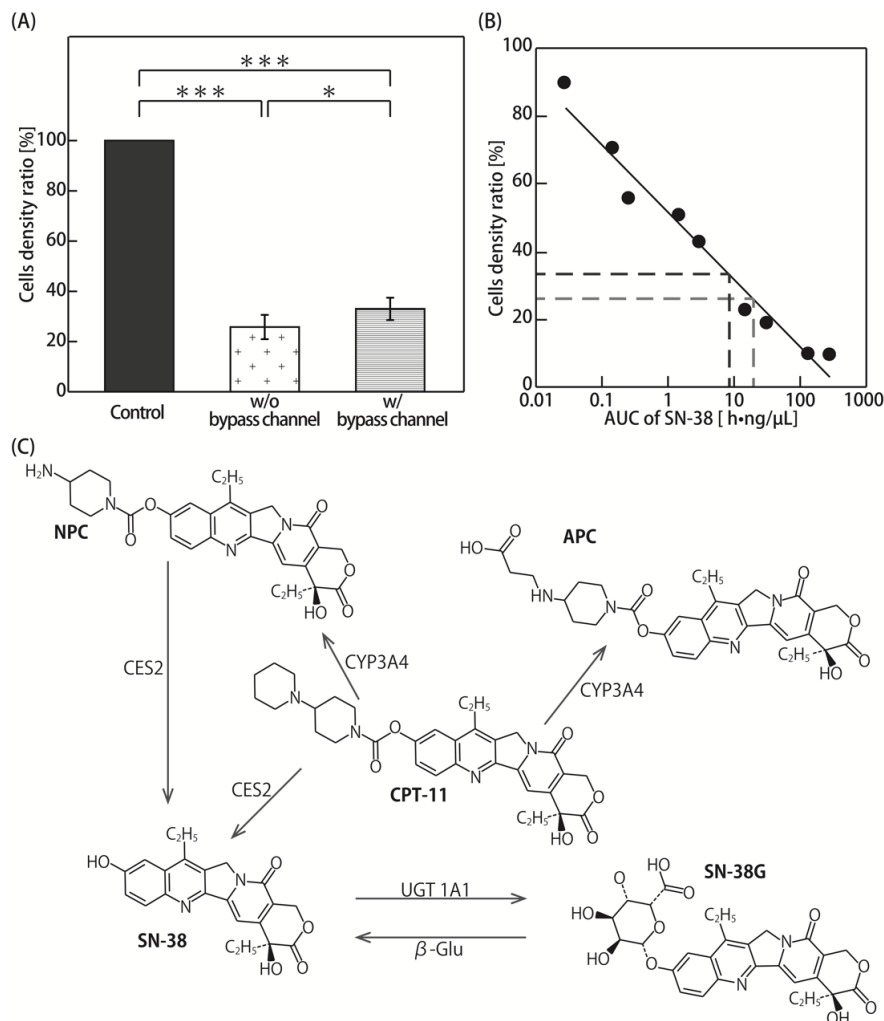


Figure 3. Evaluation of the drug efficacy in the MO-MPS. (A) Cell density ratio of A549. The cell densities are expressed as a ratio of cell density to cell density of control (n=3 to 6; mean ± S.D.). Asterisks indicate significant differences (* P < 0.05; *** P < 0.005). (B) Cell density ratio as a function of AUC of SN-38. The dark broken line indicates the result of the MO-MPS with the bypass channel, whereas the light broken line shows the result of the MO-MPS without the bypass channel. (C) Metabolic map of CPT-11 *in vivo*. CPT-11 is metabolized to APC and NPC by CYP3A4. CPT-11 and NPC are metabolized to SN-38 by CES2. SN-38 and SN-38G are reversibly metabolized by UGT1A1 and β-Glu.

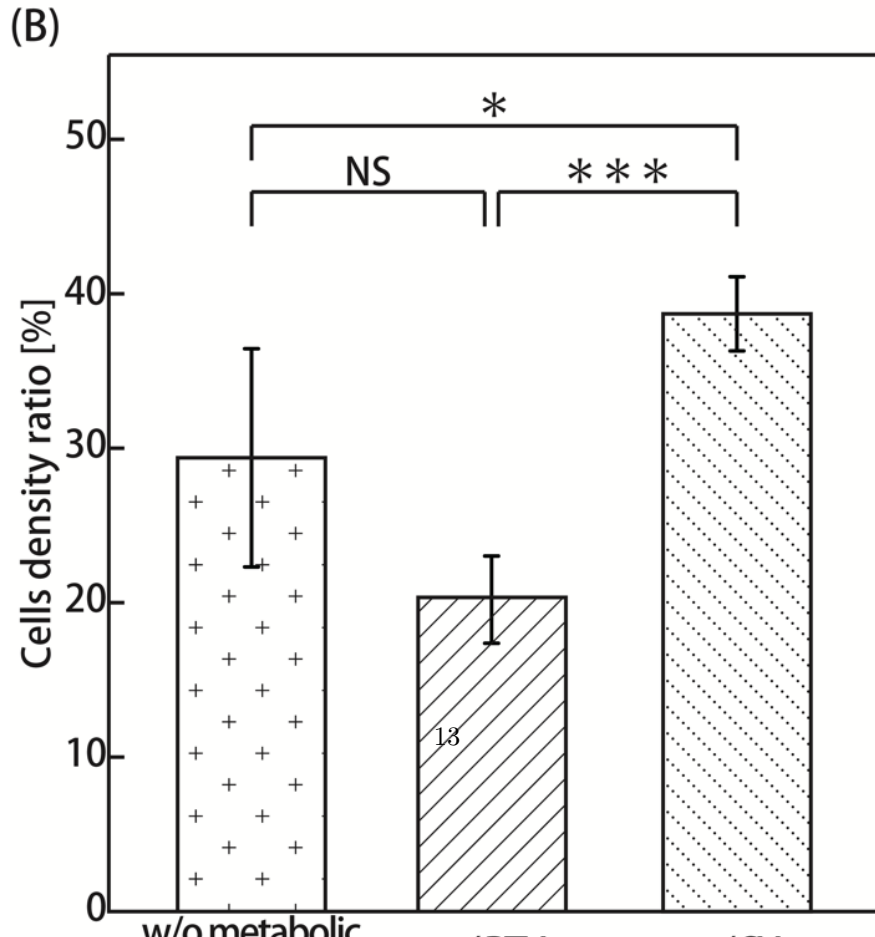
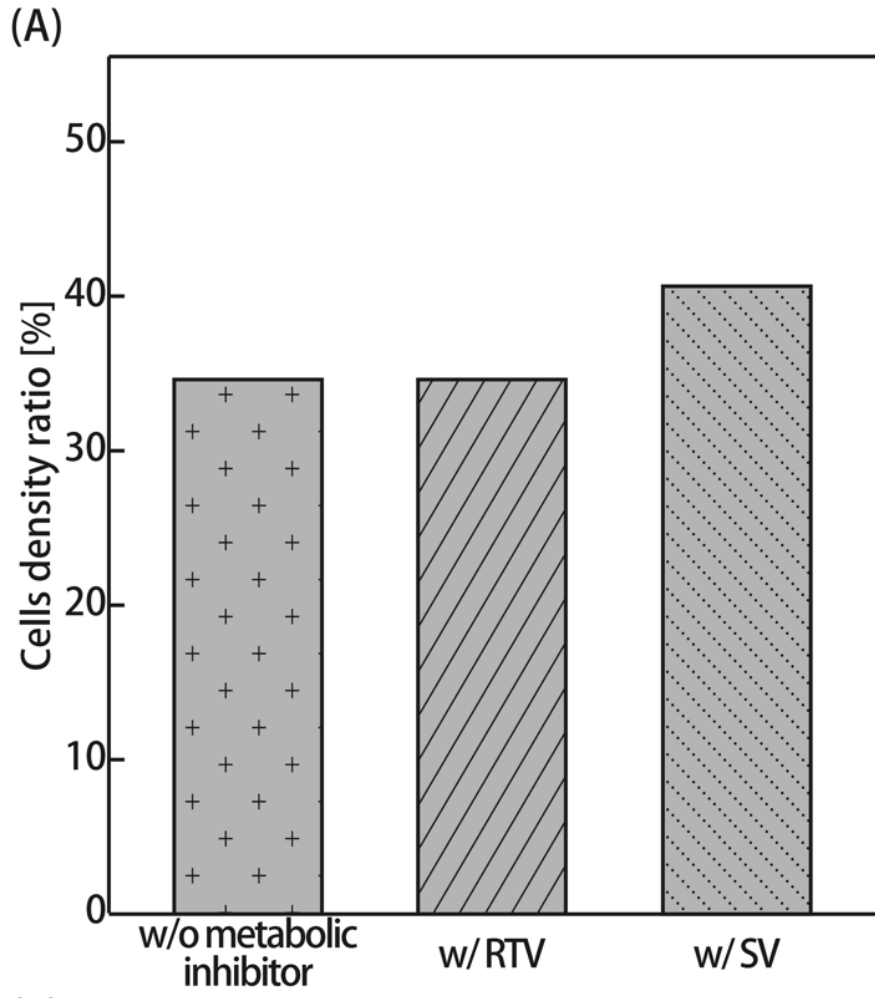


Figure 4. Evaluation of drug efficacy in concomitant administration of metabolic inhibitors. (A) Estimation results using the PK–PD model. The drug efficacies are expressed as ratios of cell density to the cell density of control. (B) Cell density ratio of A549 cells in the MO–MPS expressed as a ratio to the cell density of control experiment (n=3 or 6; mean \pm S.D.). Asterisks indicate significant differences (* P < 0.05; *** P < 0.005).